# Protein Particles in *Chlamydomonas* Flagella Undergo a Transport Cycle Consisting of Four Phases

**Carlo Iomini,* Veronica Babaev-Khaimov,* Massimo Sassaroli,‡ and Gianni Piperno***

*Department of Cell Biology and Anatomy and ‡Department of Physiology and Biophysics, Mount Sinai School of Medicine, New York, New York 10029

***Abstract.*** We used an improved procedure to analyze the intraflagellar transport (IFT) of protein particles in *Chlamydomonas* and found that the frequency of the particles, not only the velocity, changes at each end of the flagella. Thus, particles undergo structural remodeling at both flagellar locations. Therefore, we propose that the IFT consists of a cycle composed of at least four phases: phases II and IV, in which particles undergo anterograde and retrograde transport, respectively, and phases I and III, in which particles are remodeled/exchanged at the proximal and distal end of the flagellum, respectively. In support of our model, we also identified 13 distinct mutants of flagellar assembly (*fla*), each defective in one or two consecutive phases of the IFT cycle. The phase I-II mutant *fla10-1* revealed that cytoplasmic dynein requires the function of kinesin II to participate in the cycle. Phase I and II mutants accumulate complex A, a particle component, near the basal bodies. In contrast, phase III and IV mutants accumulate complex B, a second particle component, in flagellar bulges. Thus, *fla* mutations affect the function of each complex at different phases of the cycle.

Key words: intraflagellar transport • transport cycle • *Chlamydomonas* • temperature-sensitive mutants • kinesin II

## *Introduction*

The intraflagellar transport (IFT)[1] of protein particles along *Chlamydomonas* flagella was observed for the first time in paralyzed flagella mutants by video-enhanced differential interference contrast (VE-DIC) microscopy (Kozminski et al., 1993). It was the third type of flagellar motility detected in *Chlamydomonas*, in addition to the flagellar beating, which propels the cell body, and the protein movement that occurs within the flagellar membrane (Bloodgood, 1977; Goodenough and Jurivich, 1978). The IFT involves the movement of 100–200-nm-long arrays of protein complexes, referred to as "rafts" or protein particles, within the space between the membrane and the outer doublet microtubules (Kozminski et al., 1995).

The main function of the IFT is likely to be the delivery of axonemal substructures from the basal body region to the distal end of the flagellum, where the axoneme assembles (Johnson and Rosenbaum, 1992; Piperno et al., 1996). The first evidence supporting this hypothesis was obtained by the analysis of *fla10-1*, a temperature sensitive (ts) mutant for flagellar assembly that is defective in kinesin homologue protein (KHP)1 (Walther et al., 1994), one of the ATP-binding subunits of the heterotrimeric kinesin II (Scholey, 1996). In *fla10-1* shifted to the restrictive temperature, flagella shorten and proteins of IFT particles disappear from these flagella (Piperno and Mead, 1997). Other defects of *fla10-1* flagella, such as the inability to mate at the restrictive temperature (Piperno et al., 1996), may also depend on the IFT. Flagellar membrane proteins, which are required for mating (Goodenough and Jurivich, 1978), may not be transported or maintained at the distal end of flagella in the absence of IFT.

*fla10-1* and other *fla* mutants (Huang et al., 1977; Adams et al., 1982; Ramanis and Luck, 1986; Piperno et al., 1998) were also used to identify components of IFT particles. Similarly to kinesin II in *fla10-1* flagella, two distinct 17S protein complexes composed of >15 polypeptides and referred to as IFT complexes A and B were reduced in concentration in flagella of *fla* mutants at the restrictive temperature (Cole et al., 1998; Piperno et al., 1998). A second motor involved in the transport of the particles, cytoplasmic dynein, was identified with the analysis of nonconditional mutants characterized by short flagellar stumps filled with protein particles (Pazour et al., 1998, 1999; Porter et al., 1999).

Knowledge of the subunit composition of kinesin II, complexes A and B, and cytoplasmic dynein was instrumental in identifying the IFT in cilia of sea urchin (Morris

Address correspondence to Gianni Piperno, Department of Cell Biology and Anatomy, Mount Sinai School of Medicine, 1 Gustave L. Levy Pl., Box 1007, New York, NY 10029. Tel.: (212) 241-0773. Fax: (212) 860-1174. E-mail: piperno@msvax.mssm.edu

[1]*Abbreviations used in this paper:* Ab, antibody; DHC, dynein heavy chain; IFT, intraflagellar transport; KHP, kinesin homologue protein; ts, temperature-sensitive; VE-DIC, video-enhanced differential interference contrast.

and Scholey, 1997), *Caenorhabditis elegans* (Orozco et al., 1999), *Tetrahymena* (Brown et al., 1999), and mouse (Marszalek et al., 1999; Takeda et al., 1999). Although each of these systems is relevant for studying specific aspects of the IFT, only *Chlamydomonas* flagella and *C. elegans* sensory cilia are amenable to in vivo analysis of IFT by VE-DIC (Kozminski et al., 1993; Piperno et al., 1998) or fluorescence microscopy (Orozco et al., 1999). These methods have been used to dissect the mechanism of IFT at the molecular level (Piperno et al., 1998; Signor et al., 1999).

Despite the identification of molecular components of the IFT particles, our understanding of the IFT remains limited. The functions of complexes A and B as well as the contribution of basal bodies and distal structures of flagella (Dentler and Rosenbaum, 1977) to the mechanism of the IFT have not been identified.

To identify the function of proteins participating in the IFT mechanism, we have adopted an approach that investigates all components of the machinery, including IFT particles and stationary elements, such as axonemes, basal bodies, and the distal structures of flagella. We analyze the IFT in *fla* mutants that, like *fla10-1*, display normal flagella at the permissive temperature of 21°C, but disassemble them when shifted to the restrictive temperature of 32°C (Huang et al., 1977; Adams et al., 1982; Ramanis and Luck, 1986; Piperno et al., 1998). Each of these *fla* mutants may be defective in the particles, one of the motors, or one of the stationary structures of the flagellar apparatus, each mutation having a distinct effect on the IFT (Piperno et al., 1998).

To classify *fla* mutations affecting individual components of the IFT machinery, we have formulated and tested a model of the IFT process. This model is based on the notion that protein subunits of the IFT particles participate in multiple cycles of transport rather than being synthesized, used once, and degraded. Two lines of evidence suggest that such recycling indeed must occur. First, particles exchange within minutes between the cell body and flagella, even though they constitute as much as 2–4% of the flagellar protein mass (Piperno and Mead, 1997). Second, flagella regenerate from the cell body within 1 h after amputation, even in the absence of protein synthesis (Rosenbaum et al., 1969).

We report here the results of our investigation aimed at (a) providing evidence in support of the model of the IFT cycle and (b) identifying mutants with IFT defects among the *fla* mutants that we as well as others have isolated. To reach these goals we have improved our previously described method of quantitative analysis of IFT (Piperno et al., 1998). Unlike previous procedures, which measured reliably only particle velocities (Kozminski et al., 1993; Piperno et al., 1998; Orozco et al., 1999), this method also yields accurate values of the frequencies of anterograde and retrograde particles, i.e., their number per unit time.

Consequently, we have been able to demonstrate quantitatively that retrograde particles are more numerous than anterograde particles in flagella of wild-type–like cells. Interestingly, we have also identified *fla* mutants in which the frequency of retrograde particles is lower than that of anterograde particles. These observations and the evidence for particle recycling outlined above lead us to propose that, in addition to bidirectional transport, the IFT particles must also undergo a process of remodeling at both the distal and proximal ends of the flagellum. These transport and remodeling events define a model of the IFT cycle consisting of at least four phases. The identification of *fla* mutants defective in one or two consecutive phases of IFT supports this model and provides useful insights into various aspects of the IFT mechanism.

## Materials and Methods

### Strains and Genetics

Procedures for mutagenesis and screening of ts *fla* mutants have been described previously (Huang et al., 1977; Adams et al., 1982; Piperno et al., 1998). Recombinants were isolated as described (Harris, 1989). Some of the crosses were obtained under conditions used to mate *imp* impotent mutants (Pasquale and Goodenough, 1987). Two mutations were considered alleles or closely linked if they did not recombine in at least 100 zygotes.

Our present collection consists of 24 ts *fla* mutants, including nine mutants, *fla1-1*, *fla2*, *fla4*, *fla5*, *fla8*, *fla9*, *fla10-1*, *fla11*, and *fla12*, isolated by others (Huang et al., 1977; Adams et al., 1982; Ramanis and Luck, 1986), as well as 15 mutants isolated by us (Piperno et al., 1998). After the initial characterization, we identified the mutants of the second group with sequential numbers from *fla15* to *fla29*, although we did not know if they represented new loci. Other mutants characterized previously (Adams et al., 1982), *fla3*, *fla6*, *fla7*, and *fla13*, were not analyzed further because *fla3*, *fla6*, and *fla13* had lost their ts *fla* phenotype, whereas *fla7* was identified as a *fla10* allele (Lux and Dutcher, 1991).

The recombination analysis of five subsets of *fla* mutants defective in one or two successive phases of the IFT cycle (see Table III) revealed that *fla19*, *fla20*, *fla23*, *fla25*, *fla26*, and *fla29* are putative alleles of *fla1-1*. For this reason, these mutants are now identified as *fla1-2*, *fla1-3*, *fla1-4*, *fla1-5*, *fla1-6*, and *fla1-7*, respectively. *fla17-2*, a mutant allele of or closely linked to *fla17-1*, was described previously (Piperno et al., 1998).

### Motion Analysis of IFT Particles

VE-DIC microscopy, as well as acquisition and storage of video image sequences, was carried out as described previously (Piperno et al., 1998). Image processing, including the extraction of the light intensity profiles, or linescans, along the flagellum and the application of singular value decomposition and principal component analysis to suppress background noise, was also performed as described previously (Piperno et al., 1998). However, the values of seven, rather than five, pixels across the width of the flagellum were averaged for each corresponding value in the linescan, thus encompassing almost the full width of the flagellum. The method for the visualization of the linescan data was also modified. Rather than generating composite plots of offset and stacked lines, we added a procedure to scale and convert the linescan data into an 8-bit gray-scale image for printing or saving as a standard TIFF file. The scaling factor was set so that the half-range of the scaled pixel values was $\leq$3.5 standard deviations of the original pixel distribution and at least 20 pixels in the scaled image had values of 0 or 255. This scaling procedure served to eliminate extremely low and high pixel values and to increase the contrast in the processed image. Following previous reports (Mallavarapu et al., 1999; Tigges et al., 1999), we refer to these plots as kymograms and to the method as digital kymography.

Since digital kymography of particle motion requires paralyzed and straight flagella, recombinant strains between each of the *fla* mutants and a paralyzed flagella (*pf*) mutant, such as *pf15*, a mutant of the central complex, were used. It should be noted that the velocity values for *pf15*, *pf15fla10-1*, *pf15fla15*, *pf15fla16*, and *pf15fla17-1* listed in Table I and II are lower than those reported previously (Piperno et al., 1998). This discrepancy is due to a 26% overestimation of the distance per pixel in our previous report.

### Antibodies to Subunits of the IFT Particles

To obtain polyclonal antibodies (Abs) and monoclonal Abs (mAbs) to subunits of the IFT particles, single polypeptides or groups of polypeptides from the 17S complexes (Piperno and Mead, 1997) were isolated by gel electrophoresis and eluted by maceration of the polyacrylamide gel. Purified proteins were injected into Balb/c mice. Hybridoma clones were selected from individual colonies grown on soft agar.

The specificity of the Abs was determined by Western blots of one- and two-dimensional gels that resolve the polypeptides of 17S complexes from

*Table I. Velocity of Particles Undergoing Anterograde and Retrograde IFT in pf-fla Recombinants*

| Mutants | *n** | Anterograde velocity | Retrograde velocity |
|---|---|---|---|
| | | *μm/s* | *μm/s* |
| *pf15* | 56 | 1.8 (0.3)‡ | 3.1 (0.5) |
| *pf15fla15* | 18 | 1.7 (0.3) | 2.6 (0.4) |
| *pf15fla16* | 27 | 1.6 (0.2) | 2.2 (0.5) |
| *pf15fla17-1* | 19 | 1.5 (0.3) | 2.0 (0.5) |
| *pf18* | 6 | 2.0 (0.4) | 3.7 (0.6) |
| *pf18fla15* | 5 | 1.7 (0.3) | 2.2 (0.3) |
| *pf18fla16* | 4 | 2.0 (0.2) | 2.9 (0.4) |
| *pf18fla17-1* | 8 | 1.9 (0.2) | 2.5 (0.4) |
| *pf14* | 8 | 2.2 (0.2) | 3.7 (0.6) |
| *pf14fla15* | 9 | 2.0 (0.2) | 2.8 (0.6) |
| *pf14fla16* | 6 | 1.7 (0.2) | 2.5 (0.5) |
| *pf14fla17-1* | 5 | 1.8 (0.2) | 2.3 (0.5) |

*Number of cells analyzed.
‡Numbers within parentheses are standard deviations.

the flagellar matrix. Each mAb identifies a major spot in the Western blot of a two-dimensional gel corresponding to subunit p148 of complex A and subunits p81 and p71 of complex B (Piperno et al., 1998). The polyclonal Ab specific for p148 and p127 of complex A identifies the two corresponding bands in the Western blot of a one-dimensional gel (Piperno et al., 1998).

### *Immunofluorescence Microscopy of the Flagellar Apparatus*

To test for the accumulation of soluble components of the cytoplasmic matrix of flagella, *Chlamydomonas* cells were treated with autolytic enzymes (Harris, 1989) and the resulting protoplasts were bound to polyornithine slides and fixed in methanol at −80°C for 8 min. After rehydration in PBS (Piperno et al., 1987), the protoplasts were extracted by a 90-s exposure to 1% Triton X-100 in PBS, rinsed three times for 5 min with PBS, and finally incubated with primary and secondary Abs for 1 h each. The secondary Ab was FITC-labeled goat anti–mouse IgG (GIBCO BRL). Slides were mounted in Vectashield (Vector Laboratories). Microscopy was performed with a UV confocal laser scanning microscope (TCS-SP; Leica) in an inverted configuration.

### *Statistical Data Analysis*

Data are presented as mean ± SD. Data sets were compared by the Student's two-tailed unpaired *t* test using a commercial software package (Excel; Microsoft) and judged to be significantly different for values of $P < 0.01$.

Cluster analysis was performed using R, an open source system for statistical analysis and graphics, and the R version of the software package Cluster (Struyf et al., 1996). Both can be downloaded freely from http://cran.r-project.org/. Three of the six clustering functions available in the package were used: the partitioning around medoids (PAM) function, which implements the partitioning around medoids algorithm, the agglomerative hierarchical function agglomerative nesting (AGNES), and the divisive hierarchical function divisive analysis (DIANA). An in-depth description of these methods can be found in Kaufman and Rousseeuw (1990).

To calculate the optimal partition or hierarchical tree, all three methods rely on the dissimilarity or distance matrix, which contains the pairwise distance between all objects. Distances were computed using both the euclidean and the manhattan metrics (Kaufman and Rousseeuw, 1990). The results of the clustering were qualitatively independent of the metric used. Since the three variables, anterograde and retrograde velocities and frequency ratio, had different units and ranges, measurements for each variable were standardized by subtracting the variable's mean value and dividing by the variable's mean absolute deviation. This ensured that all variables were given similar weight in the calculation of the dissimilarity matrix.

Although the two hierarchical functions do not require any user input, the function PAM must be given the number of clusters into which the objects are to be divided. The quality of the clustering structure can be assessed by the overall average silhouette coefficient. For each object, the silhouette coefficient compares the average dissimilarity with the other members of its own cluster to the average dissimilarity with the objects in the closest of the other clusters. Thus, it is a measure of the strength of each object's membership to its cluster. The best clustering solution was found by invoking the function with different numbers of clusters and selecting the one giving the highest overall average silhouette coefficient.

*Table II. Velocity, Frequency Ratio, and Frequency of Particles Undergoing Anterograde and Retrograde IFT in Recombinants between pf15 and fla Mutants*

| Mutants | *n** | Anterograde velocity | Retrograde velocity | Frequency ratio‡ | Frequency |
|---|---|---|---|---|---|
| | | *μm/s* | *μm/s* | | *p/s*§ |
| 21°C | | | | | |
| *pf15* | 56 | 1.8 (0.3)‖ | 3.1 (0.5) | 0.8 (0.1) | 3.8 (1.0) |
| Phase I | | | | | |
| *pf15fla8* | 19 | 1.6 (0.3) | 3.5 (0.6) | 0.5 (0.1) | 2.4 (0.9) |
| *pf15fla10-1* | 13 | 1.4 (0.2) | 3.3 (0.4) | 0.6 (0.1) | 3.0 (0.8) |
| *pf15fla27* | 31 | 1.7 (0.3) | 3.4 (0.6) | 0.5 (0.2) | 3.1 (1.3) |
| Phase I-II | | | | | |
| *pf15fla1-1* | 11 | 1.2 (0.3) | 3.3 (0.7) | 0.4 (0.1) | 2.1 (0.7) |
| *pf15fla18* | 14 | 1.0 (0.1) | 3.0 (0.5) | 0.5 (0.2) | 2.8 (0.6) |
| *pf15fla28* | 17 | 1.1 (0.2) | 2.9 (0.4) | 0.5 (0.1) | 4.0 (1.4) |
| Phase III-IV | | | | | |
| *pf15fla2* | 13 | 1.6 (0.2) | 1.3 (0.3) | 1.5 (0.5) | 2.5 (0.6) |
| *pf15fla11* | 28 | 1.5 (0.4) | 2.3 (0.7) | 1.4 (0.4) | 1.6 (0.6) |
| *pf15fla15* | 18 | 1.7 (0.3) | 2.6 (0.4) | 1.6 (0.2) | 2.2 (1.1) |
| *pf15fla16* | 27 | 1.6 (0.2) | 2.2 (0.5) | 1.7 (0.8) | 2.2 (0.8) |
| *pf15fla17-1* | 19 | 1.5 (0.3) | 2.0 (0.5) | 1.4 (0.4) | 2.3 (1.1) |
| *pf15fla24* | 16 | 1.6 (0.2) | 0.9 (0.2) | 1.4 (0.3) | 2.3 (0.7) |
| Phase ? | | | | | |
| *pf15fla4* | 19 | 1.7 (0.2) | 2.8 (0.4) | 0.8 (0.3) | 3.0 (0.9) |
| *pf15fla5* | 19 | 1.7 (0.2) | 2.7 (0.5) | 0.8 (0.1) | 3.1 (0.9) |
| *pf15fla9* | 15 | 1.9 (0.2) | 3.1 (0.5) | 0.8 (0.1) | 2.4 (0.8) |
| *pf15fla12* | 16 | 2.2 (0.3) | 3.7 (0.6) | 0.8 (0.1) | 5.3 (0.7) |
| *pf15fla21* | 14 | 1.7 (0.2) | 2.8 (0.3) | 0.8 (0.1) | 4.2 (1.1) |
| 32°C | | | | | |
| *pf15* | 6 | 1.9 (0.2) | 3.1 (0.5) | 0.8 (0.1) | 4.7 (0.4) |
| Phase I-II | | | | | |
| *pf15fla10-1* | 13 | 1.2 (0.2) | 3.1 (0.5) | 0.5 (0.1) | 1.4 (0.7) |
| Phase IV | | | | | |
| *pf15fla4* | 9 | 1.6 (0.2) | 2.6 (0.4) | 0.7 (0.2) | 2.6 (0.6) |

In phase I, retrograde particles exchange proteins within the cell body cytoplasm and/or are remodeled into anterograde particles with a concurrent change in number around the basal body of the flagellum. In phase II, particles move from the base to the distal end of the flagellum with a characteristic velocity. In phase III, anterograde particles are remodeled into retrograde particles at the distal end of the flagellum with a concurrent change in number. Finally, in phase IV, particles move from the distal end back to the region around the basal body of the flagellum with a different velocity than that of anterograde particles.
*Number of cells analyzed.
‡Frequency ratio of particles undergoing anterograde and retrograde IFT.
§Particles per second.
‖Numbers within parentheses are standard deviations.

### *Other Procedures*

Cell culture, $^{35}$S-labeling of proteins, isolation of 17S complexes from the cytoplasmic matrix of flagella, gel electrophoresis, and Western blots were performed as described previously (Piperno et al., 1998).

## *Results*

### *Protein Subunits of the IFT Particles Are Recycled*

To obtain further evidence supporting the hypothesis that protein subunits of IFT particles are recycled, we exposed *pf15* cells to 60 μM anisomycin for 6 h and recorded the IFT by VE-DIC microscopy. Under these conditions, in which protein synthesis is inhibited by ~95% (Luck et al., 1977), the IFT continued and was indistinguishable from that observed in the absence of anisomycin (see Fig. 1 b).

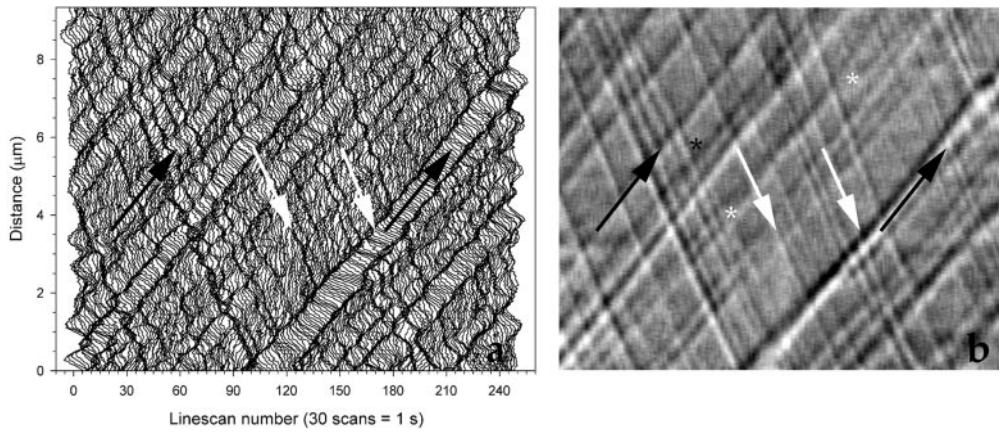


*Figure 1.* Digital kymography identifies particles undergoing IFT along one flagellum of a *Chlamydomonas pf15* mutant cell. Light intensity profiles, or linescans, were measured along the flagellum in a sequence of VE-DIC images. The same data were processed and plotted as described either in Piperno et al. (1998) (a) or in Materials and Methods (b). Vertical and horizontal axes report distance from the cell body in micrometers and time of observation, respectively, 1 s being equivalent to 30 video frames or linescans. IFT particles are seen as streaks (a) and shaded relief-like traces (b). Anterograde and retrograde particles form acute and obtuse angles, respectively, with the bottom horizontal axis. Black and white arrows indicate traces formed by the same anterograde or retrograde IFT particles, respectively, in both panels. The sudden appearance (marked by a black asterisk) or disappearance of a trace is probably due to a particle moving in or out, respectively, of the microscope focal plane. The two white asterisks mark points where two traces appear to merge and separate again. This event probably occurs when a faster particle (lower trace at early times) reaches a slower one (upper trace at early time) (lower left, white asterisk) and then surpasses it (upper right, white asterisk).

Similarly, flagellar regeneration occurs within 1 h after amputation in the absence of protein synthesis (Rosenbaum et al., 1969). This evidence, in addition to the observation that subunits of the particles turn over within minutes between cell bodies and flagella (Piperno and Mead, 1997), suggests that IFT particles undergo repeated cycles of transport in and out of flagella.

### *The IFT Cycle Consists of Four Phases*

To determine whether particles undergo a cycle consisting of more than the two phases of anterograde and retrograde transport, we have developed an improved digital kymographic analysis of VE-DIC microscopy images of flagella (Piperno et al., 1998). This method increases the sensitivity of particle detection, yielding reliable measurements of the frequency ratio of anterograde and retrograde particles that could not be obtained by previous procedures (Kozminski et al., 1993; Orozco et al., 1999).

The results of our original and current methods, applied to the same data set, are compared in Fig. 1, a and b, respectively. The particle tracks along a flagellum of *pf15*, a paralyzed flagella mutant, are visible as streaks (Fig. 1 a) and relief-like shaded traces (Fig. 1 b). In the kymograms, anterograde and retrograde particles give rise to traces forming acute and obtuse angles, respectively, with the bottom horizontal axis (Fig. 1 b). The slope of each trace yields the velocity of the particle, whereas the ratio of the number of traces and the time of observation yields the frequency of transport. All traces in Fig. 1 b are continuous and without significant changes in slope, indicating that particles did not arrest or accumulate along this representative *pf15* flagellum. Occasionally, individual particles suddenly materialize (Fig. 1 b, black asterisk) or vanish in the middle of a flagellum. Other times, two particles appear to merge and separate again (Fig. 1 b, white asterisks). The first effect results from particles moving in or out of the very shallow focal region defined by high numerical aperture DIC microscopy. The second effect occurs when a faster particle, traveling on one side of the flagellum, reaches and surpasses a slower particle moving in the same direction along a different path.

In our analysis of 56 *pf15* flagella (Table II) we identified 518 anterograde and 641 retrograde particles, each of which was included in the calculation of the respective average velocity. This expanded kymographic analysis confirmed that the velocity of anterograde particles is lower than that of retrograde particles, as reported previously for this and other *pf* mutants (Kozminski et al., 1993; Piperno et al., 1998). Although the overall particle frequency fluctuated substantially from cell to cell, the anterograde-to-retrograde particle frequency ratio was much less variable and consistently lower than one. This new quantitative result clearly demonstrates that in *pf15* retrograde particles are more numerous than anterograde ones. It also suggests that the mechanisms that regulate particle assembly/remodeling at each flagellar end may operate regardless of the conditions that determine the overall rate of IFT.

This combined evidence indicates that the IFT cycle consists of at least four phases. In phase I, which takes place in the basal body region of the flagellum, anterograde particles are assembled from retrograde particles by remodeling and/or exchange of subunits with the cell body cytoplasm, with a concurrent decrease in number. In this phase, the precursors of the flagellar structures that make up the cargo are also loaded onto the particles. In phase II, the particles are transported from the base to the distal end of the flagellum by a heterotrimeric kinesin II with a velocity of ~2 μm/s. In phase III, which occurs at the distal end of the flagellum, anterograde particles are remodeled into retrograde particles with a concurrent increase in number, probably upon or after unloading their cargo. Finally, in phase IV, retrograde particles are transported by a cytoplasmic flagellar dynein from the distal end back to the basal body region of the flagellum, with a velocity of ~3 μm/s, higher than that of anterograde particles.

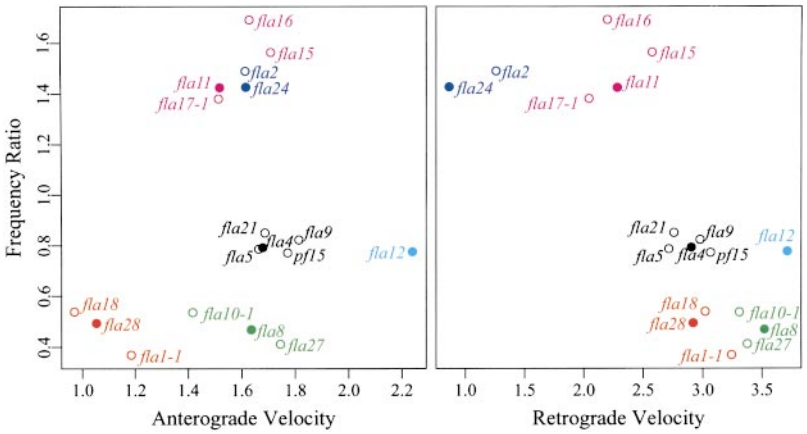


*Figure 2.* The results of the cluster analysis using the PAM program are displayed; the values of anterograde-to-retrograde particle frequency ratio are plotted as a function of anterograde and retrograde velocity. The members of each of the six clusters of mutants are identified by color. A filled circle indicates the medoid, or most representative member, of each cluster.

### *Ts Mutants of Flagellar Assembly Are Defective in One or Two Consecutive Phases of the IFT Cycle*

To identify mutants defective in distinct phases of the IFT cycle, we measured the velocity and frequency ratio of particles in flagella of *fla* mutants. For this purpose, we crossed the *fla* mutants in our collection with *pf15* and subjected the recombinants to the IFT analysis described above.

At the outset, to verify that the IFT defect in each recombinant strain is due to the *fla* mutation, we compared the effects of the *fla15*, *fla16*, and *fla17-1* mutations of retrograde IFT (Piperno et al., 1998) on the backgrounds of *pf15*, *pf18*, and *pf14*. All three *pf* mutants have long and paralyzed flagella, but *pf15* and *pf18* are mutants of the central microtubular pair complex (Adams et al., 1981), whereas *pf14* is a mutant of the radial spokes (Piperno et al., 1977). As shown in Table I, statistically significant differences exist in the values of anterograde and retrograde velocities between *pf15*, *pf18*, and *pf14*. Nevertheless, the decrease in retrograde velocity caused by each of the *fla15*, *fla16*, and *fla17-1* mutations remains evident regardless of the *pf* mutation. Thus, mutations of axonemal substructures do not qualitatively alter the defect caused by each specific *fla* mutation, although they may affect the velocities of the IFT particles.

Table II lists the results of the IFT analysis of *pf15* and of the recombinants of *pf15* with 17 *fla* mutants at the permissive temperature, as well as of *pf15*, *pf15fla10-1*, and *pf15fla4* at the restrictive temperature. By means of the analysis at the permissive temperature, we distinguished four classes of recombinants.

The first class comprises *pf15fla8*, *pf15fla10-1*, and *pf15fla27*, which display normal velocities but a lower anterograde-to-retrograde particle frequency ratio compared with *pf15.* Thus, *fla8*, *fla10-1*, and *fla27* are classified as mutants of phase I because an abnormally low number of anterograde particles are remodeled from retrograde particles or assembled de novo in the basal body region. Yet, we know that *fla10-1* is a kinesin mutant, thus a phase II mutant, as shown at 32°C.

The second class includes *pf15fla1-1*, *pf15fla18*, and *pf15fla28*, which display lower values of both particle frequency ratio and anterograde velocity than *pf15*. Thus, *fla1-1*, *fla18*, and *fla28* are identified as mutants of both assembly and transport of anterograde particles, i.e., phase I-II mutants. Six other recombinants referred to as *pf15fla1-2* to *pf15fla1-7* have values of frequency ratio and anterograde velocity similar to *pf15fla1-1*, but were not included in Table II because they are putative alleles of *fla1-1*, as reported in Materials and Methods and below.

The third class of recombinants, *pf15fla2*, *pf15fla11*, *pf15fla15*, *pf15fla16*, *pf15fla17-1*, and *pf15fla24*, is distinguished by a lower retrograde velocity and a higher particle frequency ratio than *pf15*. Thus, *fla2*, *fla11*, *fla15*, *fla16*, *fla17-1*, and *fla24* are identified as mutants of retrograde particle assembly and transport, i.e., phase III-IV mutants.

Of the remaining recombinants, *pf15fla4*, *pf15fla5*, *pf15fla9*, and *pf15fla21* display velocities, frequency ratios, and overall particle frequencies not significantly different from those of *pf15* at 21°C. The only exception is *pf15fla12*, which exhibits the highest values of anterograde and retrograde velocities and overall particle frequency among all recombinants examined. Thus, although *fla4*, *fla5*, *fla9*, *fla12*, and *fla21* may be IFT mutants, they do not present distinct defects in any phase of the cycle at the permissive temperature.

To validate this subjective classification with a more objective method, we carried out a cluster analysis of the recombinants, using the velocities and the frequency ratios as variables after standardization as described in Materials and Methods. When the function PAM was used, the best clustering structure as judged by the highest overall average silhouette coefficient was given by six clusters. The results are shown in Fig. 2, where the recombinants have been color coded according to the cluster to which they were assigned. These plots illustrate how the 17 recombinants are clearly separated into three bands based on their frequency ratios, confirming the value of this parameter for the characterization of the IFT. The class of *pf15*-like recombinants in Table II is reproduced by the black cluster, except for *pf15fla12*, which stands alone because of its extreme velocities. The phase III-IV mutants in Table II have been split into two clusters. The first, color coded in magenta, includes the recombinants with retrograde velocities of ~2 μm/s, whereas the second, color coded in blue, consists of *pf15fla2* and *pf15fla24*, whose retrograde velocities are ~1 μm/s. A similar agreement is found in the classification of the phase I and phase I-II mutants, represented by the green and red clusters, respectively. The hierarchical trees generated by functions AGNES and DIANA confirmed these results (not shown).

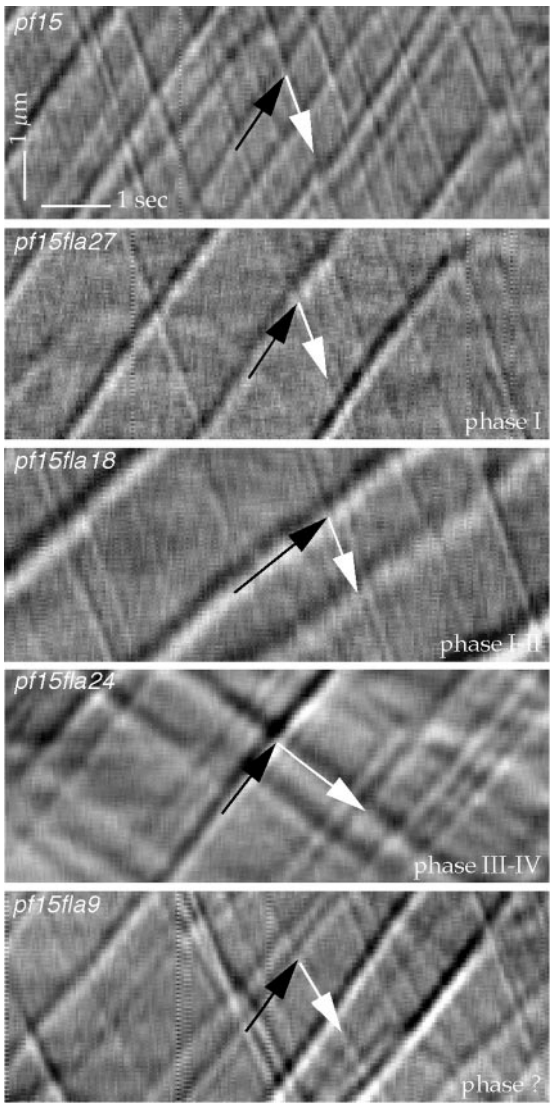


*Figure 3.* Kymograms of flagella of *pf15*, *pf15fla27*, *pf15fla18*, *pf15fla24*, and *pf15fla9*. Each recombinant is defective in one or two phases of the IFT cycle, as listed in Table II. Black and white arrows indicate traces formed by anterograde or retrograde IFT particles, respectively. Anterograde particles in *pf15fla18* and retrograde particles in *pf15fla24* are slower than in *pf15*. The apparent size of these slower particles is larger than that of the corresponding particles in *pf15*.

IFT analysis was also performed on cells incubated for 90 min at the restrictive temperature of 32°C. No moving particles were detected in flagella of *pf15fla1-1*, *pf15fla5*, *pf15fla8*, *pf15fla9*, *pf15fla15*, *pf15fla18*, and *pf15fla27*. In all other recombinants, the velocities and frequency ratios were similar to those at the permissive temperature, with the two exceptions shown in Table II. In *pf15fla10-1*, the anterograde particle velocity was significantly reduced. In contrast, in *pf15fla4*, the retrograde particle velocity decreased, whereas the frequency ratio remained *pf15*-like. Thus, after shifting to the restrictive temperature, *fla10-1* was identified as a phase I-II mutant and *fla4* as a phase IV mutant.

A typical kymogram for *pf15fla27*, *pf15fla18*, *pf15fla24*, and *pf15fla9*, each representing a different class of mutants, is shown in Fig. 3. These kymograms clearly show that the overall particle frequency in all these recombinants is lower than in *pf15* and that the anterograde particles in the phase I-II mutant *pf15fla18* and the retrograde particles in the phase III-IV mutant *pf15fla24* are slower than in *pf15*. Moreover, they illustrate the inverse correlation between the anterograde or retrograde velocity and the width of the respective particle traces. This relation was observed in every *fla* mutant examined.

### *Recombination Analyses of fla Mutations*

A recombination analysis was carried out to determine whether the *fla* mutations in each class represented independent loci. After crossing all mutants within each class, this analysis showed that they all represented independent loci, with the exception of phase I-II mutants *fla1-2* to *fla1-7*, which were identified as putative alleles of *fla1-1*.

To determine the number of independent loci represented by all *fla* mutations in our collection, the recombination analysis was extended to all *fla* mutants except the alleles of *fla1-1*, *fla17-1*, and *fla10-1*. The results reported in Table III indicate the existence of eight loci, *FLA15*, *FLA16*, *FLA17*, *FLA18*, *FLA21*, *FLA24*, *FLA27*, and *FLA28*, in addition to the nine loci represented by *fla1-1*, *fla2*, *fla4*, *fla5*, *fla8*, *fla9*, *fla10-1*, *fla11*, and *fla12*, which were previously identified (Adams et al., 1982; Ramanis and Luck, 1986). No alleles were found among mutants belonging to different classes identified by IFT analysis at 21°C.

### *Distinct IFT Defects Cause Accumulation of Particle Components at a Flagellar Extremity*

To identify defects in the localization of particles in mutants of the IFT cycle, we examined the *fla* mutants at the permissive and restrictive temperatures by immunofluorescence microscopy. A polyclonal Ab against subunits p148 and p127 of complex A and a mAb against subunit p81 of complex B were used.

Illustrations of this analysis performed on phase I-II mutants *fla10-1* and *fla1-2* and phase III-IV mutants *fla15* and *fla17-1* are shown in Fig. 4. Subunits of complex A accumulated in the basal body region in *fla1-2* and *fla10-1*. In contrast, p81 of complex B accumulated at the distal end or in bulges of flagella in *fla15* and *fla17-1*, as well as in *fla11*, *fla16*, and *fla24* (not shown). The temperature shift enhanced the defects in *fla10-1* and *fla1-2*, but not in *fla15* and *fla17-1 (*Fig. 4, right).

No flagellar immunostaining was detected after the application of (a) mAb against p81 of complex B to *fla10-1* and *fla1-2*, (b) Ab against p148 and p127 of complex A to *fla11*, *fla15*, *fla16*, *fla17-1*, and *fla24*, and (c) of both Abs to a wild-type strain (not shown). Finally, none of the remaining *fla* mutants displayed an immunofluorescence signal under our conditions.

To test whether subunits of either complex accumulate in these *fla* mutants at a level not detected by immunofluorescence, we determined the relative concentration of these polypeptides by Western blots of equal amounts of flagellar proteins developed with Abs against subunits of each complex.

No *fla* mutant displayed any accumulation of subunits of complex A in flagella. In contrast, subunits of complex B

*Table III. Recombination Analysis of fla Mutants Defective in Different Phases of the IFT Cycle*

| | *fla8* | *fla10-1* | *fla27* | *fla1-1* | *fla18* | *fla28* | *fla2* | *fla11* | *fla15* | *fla16* | *fla17-1* | *fla24* | *fla4* | *fla5* | *fla9* | *fla12* | *fla21* |
|---|---|---|---|---|---|---|---|---|---|---|---|---|---|---|---|---|---|
| Phase I | | | | | | | | | | | | | | | | | |
| *fla8* | | | | | | | | | | | | | | | | | |
| *fla10-1* | L* | | | | | | | | | | | | | | | | |
| *fla27* | 14:32 | 8:10 | | | | | | | | | | | | | | | |
| Phase I-II | | | | | | | | | | | | | | | | | |
| *fla1-1* | L | L | 11:13 | | | | | | | | | | | | | | |
| *fla18* | 0:12 | 11:13 | 8:26 | 2:18 | | | | | | | | | | | | | |
| *fla28* | 5:4 | 66:3 | 15:19 | 12:14 | 12:6 | | | | | | | | | | | | |
| Phase III-IV | | | | | | | | | | | | | | | | | |
| *fla2* | L | L | 11:9 | L | 21:25 | 13:8 | | | | | | | | | | | |
| *fla11* | L | L | 1:21 | L | 6:12 | 1:15 | L | | | | | | | | | | |
| *fla15* | 6:18 | 2:14 | 17:28 | 13:25 | 0:24 | 9:26 | 3:7 | 22:37 | | | | | | | | | |
| *fla16* | 5:12 | 2:1 | 0:16 | 0:24 | 3:16 | 6:7 | 5:4 | 0:23 | 1:2 | | | | | | | | |
| *fla17-1* | 5:8 | 0:4 | 3:17 | 2:16 | 11:5 | 4:3 | 1:22 | 0:49 | 1:7 | 0:5 | | | | | | | |
| *fla24* | 4:9 | 4:21 | 0:17 | 7:14 | 3:13 | 6:7 | 8:35 | 5:33 | 4:9 | 1:24 | 3:3 | | | | | | |
| Phase IV | | | | | | | | | | | | | | | | | |
| *fla4* | L | L | 136:5 | L | 1:26 | 10:4 | 23:9 | L | 3:17 | 2:10 | 2:5 | 37:13 | | | | | |
| Phase ? | | | | | | | | | | | | | | | | | |
| *fla5* | L | L | 3:9 | L | 3:16 | 7:8 | L | L | 2:10 | 5:16 | 4:20 | 2:18 | L | | | | |
| *fla9* | L | L | 7:16 | L | 1:15 | 16:5 | L | L | 3:17 | 2:14 | 54:1 | 15:6 | L | L | | | |
| *fla12* | L | L | 3:24 | L | 5:15 | 12:23 | L | L | 2:22 | 1:39 | 2:12 | 9:18 | L | L | L | | |
| *fla21* | 0:8 | 2:18 | 7:25 | 16:32 | 0:26 | 13:14 | 6:7 | 3:17 | 6:14 | 0:23 | 16:9 | 5:2 | 2:4 | 1:20 | 19:5 | 7:14 | |

Tetrad analysis was performed on unresolved zygospores. Therefore, each ratio represents the number of parental ditype to the number of combined tetratype and nonparental ditype.
*L indicates crosses that were analyzed by others (Adams et al., 1982; Ramanis and Luck, 1986). The mutants involved in these crosses represent different loci.

were shown to accumulate in flagella of phase III-IV mutants *fla11*, *fla15*, *fla17-1*, and *fla24*, confirming the immunofluorescence observations. A similar accumulation was also observed in flagella of the phase IV mutant *fla4*, as well as in *fla21*. Subunits of complex B were never found accumulated in flagella of phase I and I-II mutants.

One example of this assay is shown in Fig. 5. The assay was performed on flagellar proteins from a wild-type strain, the phase I mutant *fla8*, the phase I-II mutant *fla1-3*, the phase III-IV mutant *fla11*, and the mutant *fla21* using mAbs against p148 of complex A and p81 of complex B. The relative intensities of the two bands in the Western blot were similar in wild-type, *fla8*, and *fla1-3*, whereas they differed in *fla11* and *fla21*: p81 of complex B increased in concentration relative to p148 of complex A (Fig. 5 b). Analogous results were found using a polyclonal Ab to subunits p148 and

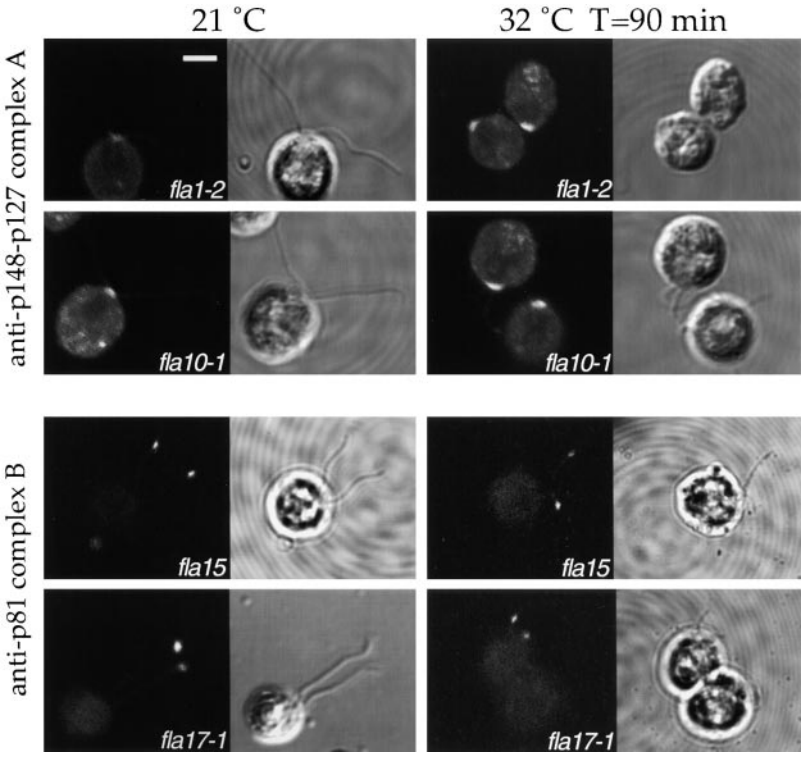


*Figure 4.* IFT particles accumulate at one of the flagellar extremities as a consequence of specific *fla* mutations. Left and right panels display cells that were incubated at the permissive temperature of 21°C or for 90 min at the restrictive temperature of 32°C. Each panel shows the same field observed by immunofluorescence, left, and phase microscopy, right. A polyclonal Ab to subunits p148 and p127 of the IFT complex A was applied to cells of *fla1-2* and *fla10-1*; an mAb to subunit p81 of the IFT complex B was applied to cells of *fla15* and *fla17-1*. Bar, 5 μm.

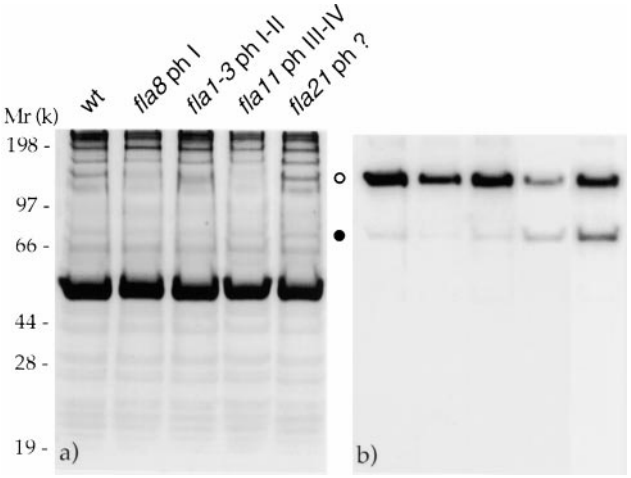


*Figure 5.* Complex B accumulates in flagella of phase III and IV mutants. Gels were loaded with equal amounts of flagellar proteins from a wild-type (wt) strain, *fla8*, *fla1-3*, *fla11*, and *fla21*. (a) The autoradiogram of $^{35}$S-labeled flagellar proteins. (b) Western blot obtained with two mAbs, one against subunit p148 of complex A and the other against p81 of complex B. Open circle, p148; filled circle, p81.

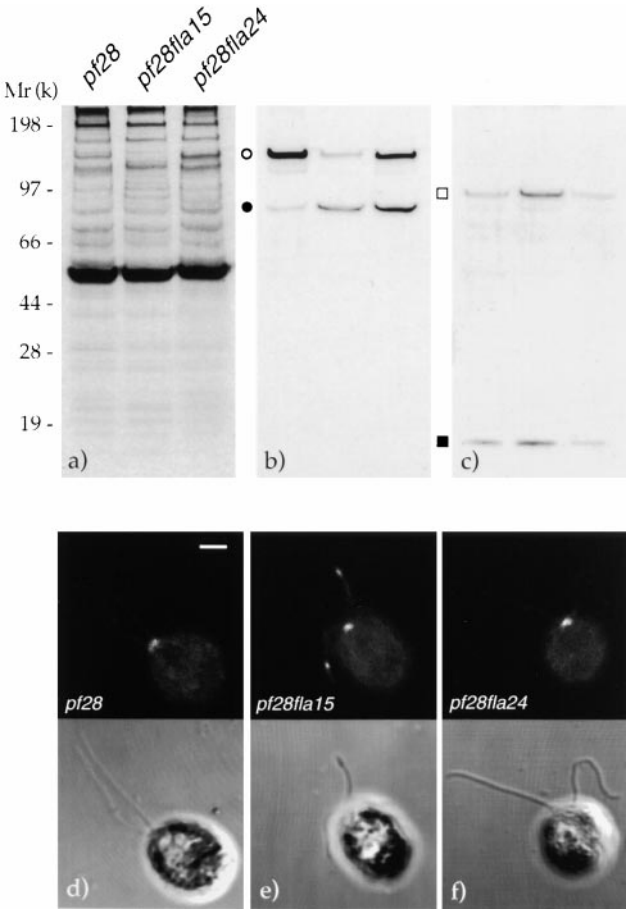


*Figure 6.* The accumulation of complex B in flagella of phase III and IV mutants does not necessarily correlate with that of cytoplasmic dynein. (a) The autoradiogram of $^{35}$S-labeled proteins resolved by gel electrophoresis. (b and c) Western blots of equal amounts of flagellar proteins from *pf28*, *pf28fla15*, and *pf28fla24* that were processed in parallel. (b) Same gel as in panel a after exposure to Abs to p148 of complex A and p81 of complex B. Open circle, p148; filled circle, p81. (c) Western blot of a gel processed in parallel and developed with Abs to KHP1 and LC7. Open square, KHP1; filled square, LC7. (d–f) Each panel displays the same field observed by immunofluorescence (top) and phase microscopy (bottom). An Ab to DHC1b was applied to cells of *pf28*, *pf28fla15*, and *pf28fla24*. Bar, 2 μm.

p127 of complex A and a mAb to p71 of complex B. Therefore, the whole complex B probably accumulates in flagella of phase III-IV mutants as well as in *fla21*.

The accumulation of complex B in flagella of phase III-IV mutants led us to investigate whether a similar behavior is shown also by the molecular motors, kinesin II and cytoplasmic dynein. This observation could provide evidence for an association between complex B and either one or both motors. Flagellar proteins from phase III-IV mutants *fla15* and *fla24* were analyzed by Western blots using Abs specific for KHP1 and LC7, subunits of kinesin II and cytoplasmic dynein, respectively, as well as mAbs against p148 of complex A and p81 of complex B. To prevent binding of anti-LC7 Ab to a light chain of outer dynein arms (Bowman et al., 1999), we used recombinants of *fla15* and *fla24* on a background of *pf28*, a strain that lacks outer dynein arms (Mitchell and Rosenbaum, 1985).

The concentration of the p81 subunit of complex B relative to that of the p148 subunit of complex A was higher in *pf28fla15* and *pf28fla24* than in *pf28* (Fig. 6 b). In addition, KHP1 and LC7 were more abundant in *pf28fla15* than in *pf28fla24* and *pf28* (Fig. 6 c). Therefore, both molecular motors accumulate in flagella of *fla15* but not of *fla24*.

To confirm this observation, we immunostained *pf28*, *pf28fla15*, and *pf28fla24* cells using Abs to LC7, KHP1, and dynein heavy chain (DHC)1b, the heavy subunit of cytoplasmic dynein. Although no immunofluorescence was detected with the Abs to LC7 or KHP1, the anti-DHC1b Ab labeled the flagellar bulges in *pf28fla15*, but not the flagella of *pf28* or *pf28fla24* (Fig. 6, d–f). In addition, cytoplasmic dynein was detected in the region near the basal bodies in all these strains, as reported previously (Pazour et al., 1999).

### *Cytoplasmic Dynein Requires the Activity of Kinesin II to Enter the Flagellum*

The concurrent increase of the concentration of subunits of kinesin II and cytoplasmic dynein in flagella of *pf28fla15* indicated that both motors undergo a process of transport in and out of flagella similar to complexes A and B. Therefore, cytoplasmic dynein, like complexes A and B, may require kinesin II to enter the flagella from the cell body.

To determine whether cytoplasmic dynein and kinesin II behave like components of the IFT particles, we tested whether exposure to 32°C would result in depletion of their subunits from flagella of *fla* mutants. For this experiment we used *fla10-1*, a point mutant in the subunit KHP1 of kinesin II (Walther et al., 1994). This mutant is defective in phases I and II of the IFT cycle and its flagella lack subunits of complexes A and B (Piperno and Mead, 1997) and IFT particles (Kozminski et al., 1995) when shifted to 32°C.

To find conditions that would preserve the flagella but lead to the depletion of particles, we analyzed the IFT in *pf15fla10-1* cells as a function of time of exposure to 32°C. After 1 h at 32°C, anterograde particles underwent a re-

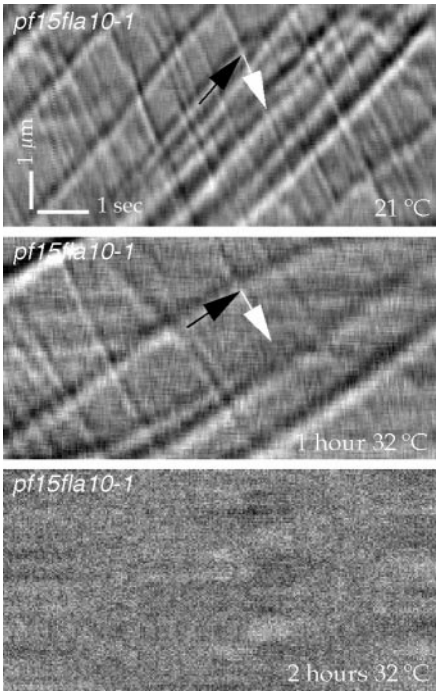


*Figure 7.* IFT is inhibited in flagella of *pf15fla10-1* exposed to the restrictive temperature. Kymograms of flagella of *pf15fla10-1* at 21°C (top) and after incubation for 1 or 2 h at 32°C (middle and bottom, respectively). No IFT particles are visible in flagella exposed to 32°C for 2 h.

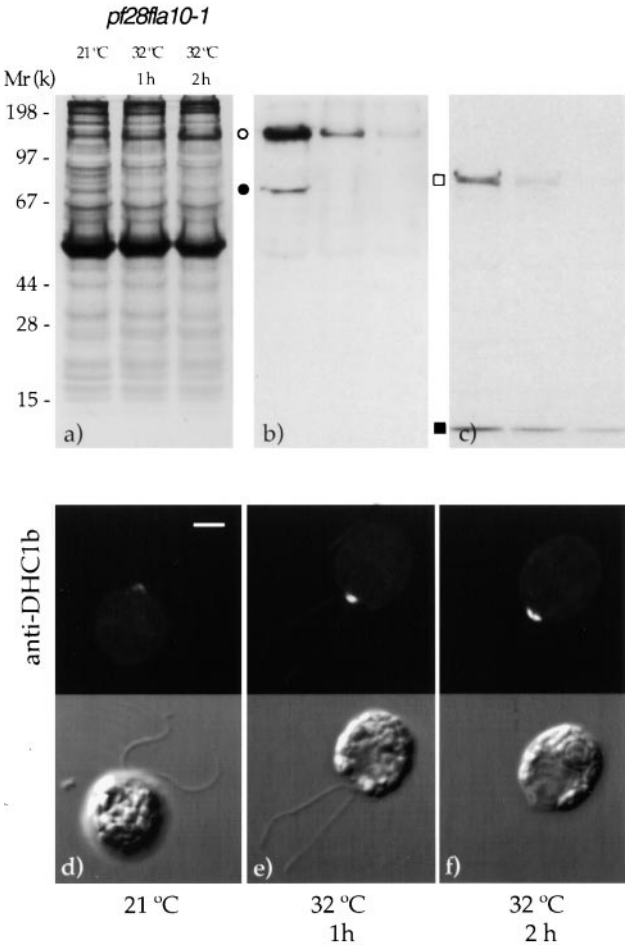


*Figure 8.* The depletion of particles from flagella of *pf28fla10-1* cells as a function of time of exposure to the restrictive temperature of 32°C correlates with the depletion of complexes A and B as well as of kinesin II and cytoplasmic dynein. (b and c) Western blots of equal amounts of flagellar proteins that were processed in parallel. (a) Autoradiogram of $^{35}$S-labeled proteins resolved by gel electrophoresis. (b) Same gel as in panel a after exposure to mAbs against subunits p148 of complex A and p81 of complex B. Open circle, p148; filled circle, p81. (c) Western blot developed using Abs to KHP1 and LC7. Open square, KHP1; filled square, LC7. (d–f) Immunofluorescence signal from an anti-DHC1b Ab applied to *pf28fla10-1* cells incubated at 21°C or at 32°C for 1 or 2 h, respectively. In each panel, the same cells are displayed as viewed by immunofluorescence (top) and phase microscopy (bottom). Bar, 2 μm.

duction in frequency and velocity and an increase in apparent size, whereas after 2 h no particles were visible (Fig. 7).

To determine whether motors and complexes were depleted from *fla10-1* in proportion to the particles, we used the Abs described above in a Western blot analysis of flagellar proteins from *pf28fla10-1* cells incubated at 21°C or at 32°C for 1 and 2 h (Fig. 8, a–c). Exposure of *pf28fla10-1* to 32°C led to progressive reduction in the concentrations of p148 of complex A and p81 of complex B (Fig. 8 b), as well as of KHP1 and LC7 (Fig. 8 c). All these antigens became either undetectable or greatly reduced in flagella of cells incubated at 32°C for 2 h. Thus, like the particles, each of these proteins requires the activity of KHP1 to enter the flagella.

Cytoplasmic dynein accumulates in the region around the basal bodies when it is not transported in flagella. This was shown in *pf28fla10-1* at both temperatures by immunofluorescence microscopy using an Ab against DHC1b (Fig. 8, d–f). Cytoplasmic dynein immunostaining was detected at 21°C and increased upon exposure of the cells to the 32°C.

## Discussion

We report that the IFT of protein particles in *Chlamydomonas* consists of a cycle composed of at least four phases. We also provide new information on the IFT mechanism by phenotypic analysis of ts mutants that are affected in one or two consecutive phases of the cycle.

### Protein Particles Carry Out the IFT in a Cycle

The IFT particles include several units of complexes A and B (Kozminski et al., 1993; Cole et al., 1998), as well as kinesin II (Signor et al., 1999) and cytoplasmic dynein (this report). In addition, the particles may include precursors of axonemal substructures (Piperno and Mead, 1997), which are assembled as multiprotein complexes in the cell body (Luck et al., 1977; Luck and Piperno, 1989) and are transported to their site of function in the flagellum by the IFT machinery.

The particles continue to carry out the IFT for several hours in the absence of protein synthesis, although they turnover within minutes (Piperno and Mead, 1997). This evidence suggests that they are reused multiple times rather than being hydrolyzed after each transport cycle. In agreement with this hypothesis, polypeptide components of complex B, such as p81 and p172, KHP1 of kinesin II (Cole et al., 1998), and DHC1b of cytoplasmic dynein (Pa-

zour et al., 1999) were found concentrated around the basal bodies of wild-type strains, where probably they are assembled/remodeled into anterograde particles.

Support for the hypothesis of a recycling of IFT particle components between the two ends of flagella comes from the accumulation of complex A near the basal bodies of some *fla* mutants and of complex B near the distal end of flagella of other *fla* mutants. Thus, IFT particle components proceed through the IFT cycle until they are arrested in a distinct region of the flagellum as the result of the disruption of the function of one of their subunits by a *fla* mutation. The sites where these defects are most evident are the flagellar extremities, not other parts of the flagellar apparatus, such as the cytoplasmic, single microtubules originating from the basal bodies.

### *The IFT Cycle Consists of At Least Four Phases*

To identify other phases of the IFT cycle in addition to those of anterograde and retrograde transport, we have improved a digital kymographic procedure for the analysis of particle transport based on VE-DIC microscopy. Our quantitative analysis demonstrated that the frequency of retrograde particles is higher than that of anterograde particles in strains with a normal IFT cycle. This was observed even though retrograde particles generate a much weaker DIC signature than anterograde particles and thus could be undercounted. Therefore, in addition to transport, particles must undergo remodeling at both flagellar extremities. Consequently, the IFT cycle must consist of at least four phases.

Anterograde particles are remodeled into smaller retrograde particles at the distal end of the flagellum in wild-type cells. Conversely, retrograde particles are remodeled into larger anterograde particles at the proximal end. Both processes probably proceed through dissociation and reassembly of multiple units of complexes A and B. However, in phase I forming anterograde particles may also exchange subunits with those in a pool within the cell body, thus recruiting proteins that have never participated in the IFT.

The frequency ratio of particles undergoing anterograde and retrograde IFT varies from cell to cell much less than the overall particle frequency, suggesting that the mechanisms involved in particle remodeling are distinct from those controlling the IFT rate. This hypothesis is supported by the identification of *pf15fla* recombinants with frequency ratios $\leq 0.5$ or $\geq 1.4$, but similar overall particle frequencies.

Frequency ratios above or below unity and the relative widths of the traces in the kimograms imply that anterograde and retrograde particles differ in size. This is illustrated in Fig. 3, where in *pf15fla24* retrograde particles generate wider traces than anterograde particles. In contrast, the traces of retrograde particles are narrower than the traces of anterograde particles in *pf15fla27*, *pf15fla18*, and *pf15fla9*. Interestingly, the anterograde-to-retrograde particle frequency ratio is 1.4 in *pf15fla24*, whereas it is $\leq 0.8$ in the others.

We also found an inverse relationship between the apparent size, as deduced from the widths of their traces, and the velocities of the particles (Fig. 3). Thus, anterograde particles are apparently larger and slower in *pf15fla18* than in all the other recombinants shown. A similar observation applies to retrograde particles in *pf15fla24*. Larger particles may experience increased frictional drag that would lower their velocity. Alternatively, slower motors, such as the mutant kinesin II in *fla10-1*, may lead to a higher degree of association of particle components and larger particles. This second hypothesis could be tested by measuring the size and frequency of anterograde particles in various *FLA10* mutants (Lux and Dutcher, 1991), provided these were found to synthesize kinesin II molecules with different intrinsic velocities.

### *The Majority of Ts Mutants of Flagellar Assembly Are Mutants in Distinct Phases of the IFT Cycle*

To identify ts mutants with defective properties of the IFT cycle, we have generated recombinants that are *fla* as well as *pf*. The flagellar paralysis necessary to carry out the VE-DIC microscopy could affect the velocities and frequencies of the IFT particles. For this reason, we have verified that the *pf15* background did not alter qualitatively the phenotypes of the *fla* mutations. With the analysis of *pf15fla* recombinants we found that the majority of the ts *fla* mutants are mutants of the IFT cycle.

Four mutants are defective only in one parameter, either the frequency ratio or one of the velocities. Nine additional mutants present defects in the frequency ratio and in one of the velocities. This is not surprising, since subunits of both molecular motors and complexes A and B are likely to participate in more than one event of the cycle. One example of this is provided by *fla10-1*, in which a point mutation in kinesin II (Walther et al., 1994) affects both the assembly of anterograde particles around the basal bodies in phase I as well as their transport velocity in phase II.

The mutants *fla5*, *fla9*, *fla12*, and *fla21* were not assigned to any phase because they were not defective in either particle velocity or frequency ratio. However, these *fla* mutants are affected in other aspects of their IFT phenotype. As compared with *pf15*, the overall particle frequency is lower in *pf15fla5* and *pf15fla9* and higher in *pf15fla12*. On the other hand, *fla21* showed an accumulation of complex B in flagella, as phase III-IV mutants do.

Our failure to identify a defective phase of the IFT cycle in these four mutants may derive from the conditions under which the IFT was observed. Perhaps these mutants do not present a defective IFT phenotype at 21°C but may acquire one upon exposure to 32°C for a sufficient time. An example of this behavior is provided by *fla4*, which was identified as a phase IV mutant only after a 90-min exposure to the restrictive temperature. Alternatively, some of these mutants are defective in the transport of components of the IFT machinery from the site of synthesis toward the basal body region. In agreement with this hypothesis, the *fla9* defect is evident only in regenerating flagella (Adams et al., 1982).

Evidence from the recombination analysis supports the validity of grouping the *fla* mutants on the basis of parameters that characterize each phase of the IFT cycle. Six alleles of *fla1-1* and one allele of *fla17-1* were uncovered by the recombination of strains within the groups comprising phase I-II and phase III-IV mutants, respectively. In contrast, no other alleles have been found in 101 crosses among all the other *fla* mutants in our collection.

Results of a cluster analysis also support the separation of *fla* mutants in four classes. In addition, this analysis in-

dicates that the phase III-IV mutants *fla11*, *fla15*, *fla16*, and *fla17-1* may be distinct from *fla2* and *fla24*, since they are defective in retrograde velocity to a lower extent. Interestingly, *fla11*, *fla15*, *fla16*, and *fla17-1* display membrane bulges at the distal end of their flagella (Piperno et al., 1998), whereas *fla2* and *fla24* do not.

### *IFT Cycle Mutants Provide Novel Insights into the Mechanism of IFT*

Evidence that a molecular motor, kinesin II, is a cargo of a flagellar cytoplasmic dynein was obtained with the analysis of the *C. elegans* mutant *che-3*, which is defective in the cytoplasmic dynein heavy chain DHC1b (Signor et al., 1999). In this mutant the retrograde transport of KAP-GFP, a green fluorescent protein–tagged accessory polypeptide of kinesin II, was inhibited in cilia but not in dendrites of sensory neurons.

Novel evidence that cytoplasmic dynein is a cargo of kinesin II is described here. Exposure of *fla10-1* to 32°C depletes flagella of cytoplasmic dynein, kinesin II, and particles. Thus, cytoplasmic dynein may be carried into the flagellum by the same kinesin II responsible for the anterograde transport of the particles in phase II.

The phenotype of most *fla* mutants differs from that of a reference strain for the accumulation of particle components in flagella or near the basal bodies. The accumulation of complex B in membrane bulges or at the distal end of flagella in phase III-IV mutants is matched by the accumulation of complex A near the basal bodies of phase I-II mutants.

The proteins accumulating at either end of mutant flagella must include the subunit whose function is affected, directly or indirectly, by the *fla* mutation. The exclusive accumulation of each complex at one location suggests that the functional role of this protein was expressed during a specific phase of the IFT cycle. Thus, for complex B to accumulate, the affected protein must be involved in the progress of the particle through phases III and IV. Conversely, for complex A to accumulate, the affected protein must be involved in the progress of the particle through phases I and II.

The mutation-dependent behavior of complexes A and B differs from that of the two motors in at least one aspect. Although complex A accumulates independently of complex B, the concentrations of kinesin II and cytoplasmic dynein vary in parallel. This implies that although complexes A and B may dissociate and reassemble during the IFT cycle, the two motors remain associated throughout the transport cycle.

The accumulation of complex A and B at the proximal and distal end, respectively, of flagella suggests that two mechanisms exist for checking the integrity of the IFT particles at each flagellar extremity. In every mutant, these putative control mechanisms maintain the assembly of the highest possible number of functional particles and their progression through the IFT phases not affected by the mutation. This is possible in ts *fla* mutants which maintain their flagella at the permissive temperature, but not in nonconditional mutants, like those lacking the cytoplasmic dynein (Pazour et al., 1999; Porter et al., 1999) which fail to assemble normal flagella.

In summary, our analysis of the IFT in *Chlamydomonas* demonstrates the existence of two phases of remodeling/assembly of IFT particles at the distal and proximal extremities of flagella, in addition to the anterograde and retrograde transport phases. It also provides new evidence that, depending on the transport phase, kinesin II and cytoplasmic dynein alternate as motor and cargo of the IFT particles. Similarly, two other particle components, complexes A and B, may switch function during distinct phases of the IFT cycle. The isolation of ts mutants defective in different phases of the cycle and the development of an improved method of IFT analysis give us the ability to investigate the function of the IFT at the molecular level.

We are grateful to Heikki Väänänen for performing all the DIC microscopy video recordings for this study and to Karla Tejada for helping with the recombination analysis of the *fla* mutants. A polyclonal Ab against KHP1, a subunit of kinesin II, was provided by Dr. John Hall, The Rockefeller University, New York, NY, and a polyclonal Ab against LC7, a subunit of cytoplasmic dynein (Bowman et al., 1999) was provided by Dr. Stephen King, University of Connecticut, Farmington, CT. A polyclonal Ab to DHC1b was provided by Drs. Gregory Pazour and George Witman, University of Massachussets Medical Center, Shrewsbury, MA. We are grateful also to Dr. Scott Henderson for his guidance in the use of the confocal microscope.

Confocal laser scanning microscopy was performed at the MSSM-CLSM core facility, supported with funding from a National Institutes of Health shared instrumentation grant (1 S10 RR0 9145-01) and a National Science Foundation Major Research Instrumentation grant (DBI-9724504). This work was supported by grant GM44467 from the National Institutes of Health, and grant 2044348 from the Consiglio Nazionale delle Recherche.

Submitted: 2 August 2000
Revised: 30 January 2001
Accepted: 30 January 2001

#### *References*

Adams, G.M., B. Huang, G. Piperno, and D.J. Luck. 1981. Central-pair microtubular complex of *Chlamydomonas* flagella: polypeptide composition as revealed by analysis of mutants. *J. Cell Biol.* 91:69–76.

Adams, G.M., B. Huang, and D.J.L. Luck. 1982. Temperature-sensitive assembly defective flagella mutants of *Chlamydomonas reinhardtii*. *Genetics.* 100: 579–586.

Bloodgood, R.A. 1977. Motility occurring in association with the surface of the *Chlamydomonas* flagellum. *J. Cell Biol.* 75:983–989.

Bowman, A.B., R.S. Patel-King, S.E. Benashski, J.M. McCaffery, L.S. Goldstein, and S.M. King. 1999. *Drosophila* roadblock and *Chlamydomonas* LC7: a conserved family of dynein-associated proteins involved in axonal transport, flagellar motility, and mitosis. *J. Cell Biol.* 146:165–180.

Brown, J.M., C. Marsala, R. Kosoy, and J. Gaertig. 1999. Kinesin-II is preferentially targeted to assembling cilia and is required for ciliogenesis and normal cytokinesis in *Tetrahymena*. *Mol. Biol. Cell.* 10:3081–3096.

Cole, D.G., D.R. Diener, A.L. Himelblau, P.L. Beech, J.C. Fuster, and J.L. Rosenbaum. 1998. *Chlamydomonas* kinesin II–dependent intraflagellar transport (IFT): IFT particles contain proteins required for ciliary assembly in *Caenorhabditis elegans* sensory neurons. *J. Cell Biol.* 141:993–1008.

Dentler, W.L., and J.L. Rosenbaum. 1977. Flagellar elongation and shortening in *Chlamydomonas*. III. Structures attached to the tips of flagellar microtubules and their relationship to the directionality of flagellar microtubule assembly. *J. Cell Biol.* 74:747–759.

Goodenough, U.W., and D. Jurivich. 1978. Tipping and mating-structure activation induced in *Chlamydomonas* gametes by flagellar membrane antisera. *J. Cell Biol.* 79:680–693.

Harris, E.H. 1989. The *Chlamydomonas* Sourcebook. Academic Press, New York. 780 pp.

Huang, B., M.R. Rifkin, and D.J. Luck. 1977. Temperature-sensitive mutations affecting flagellar assembly and function in *Chlamydomonas reinhardtii*. *J. Cell Biol.* 72:67–85.

Johnson, K.A., and J.L. Rosenbaum. 1992. Polarity of flagellar assembly in *Chlamydomonas*. *J. Cell Biol.* 119:1605–1611.

Kaufman, L., and P.J. Rousseeuw. 1990. Finding Groups in Data: an Introduction to Cluster Analysis. John Wiley & Sons, Inc., New York. 342 pp.

Kozminski, K.G., K.A. Johnson, P. Forscher, and J.L. Rosenbaum. 1993. A motility in the eukaryotic flagellum unrelated to flagellar beating. *Proc. Natl. Acad. Sci. USA*. 90:5519–5523.

Kozminski, K.G., P.L. Beech, and J.L. Rosenbaum. 1995. The *Chlamydomonas*

kinesin-like protein *Fla10* is involved in motility associated with the flagellar membrane. *J. Cell Biol.* 131:1517–1527.

Luck, D., G. Piperno, Z. Ramanis, and B. Huang. 1977. Flagellar mutants of *Chlamydomonas*: studies of radial spoke-defective strains by dikaryon and revertant analysis. *Proc. Natl. Acad. Sci. USA*. 74:3456–3460.

Luck, D.J.L., and G. Piperno. 1989. Dynein arm mutants of *Chlamydomonas*. *In* Cell Movement. F.D. Warner, P. Satir, and I.R. Gibbons, editors. Alan R. Liss, New York. 49–60.

Lux, F.G., and S.K. Dutcher. 1991. Genetic interactions at the *FLA10* locus: suppressors and synthetic phenotypes that affect the cell cycle and flagellar function in *Chlamydomonas reinhardtii*. *Genetics.* 128:549–561.

Mallavarapu, A., K. Sawin, and T. Mitchison. 1999. A switch in microtubule dynamics at the onset of anaphase B in the mitotic spindle of *Schizosaccharomyces pombe*. *Curr. Biol.* 9:1423–1426.

Marszalek, J.R., P. Ruiz-Lozano, E. Roberts, K.R. Chien, and L.S. Goldstein. 1999. Situs inversus and embryonic ciliary morphogenesis defects in mouse mutants lacking the KIF3A subunit of kinesin-II. *Proc. Natl. Acad. Sci. USA.* 96:5043–5048.

Mitchell, D.R., and J.L. Rosenbaum. 1985. A motile *Chlamydomonas* flagellar mutant that lacks outer dynein arms. *J. Cell Biol.* 100:1228–1234.

Morris, R.L., and J.M. Scholey. 1997. Heterotrimeric kinesin-II is required for the assembly of motile 9+2 ciliary axonemes on sea urchin embryos. *J. Cell Biol.* 138:1009–1022.

Orozco, J.T., K.P. Wedaman, D. Signor, H. Brown, L. Rose, and J.M. Scholey. 1999. Movement of motor and cargo along cilia. *Nature.* 398:674.

Pasquale, S.M., and U.W. Goodenough. 1987. Cyclic AMP functions as a primary sexual signal in gametes of *Chlamydomonas reinhardtii*. *J. Cell Biol.* 105:2279–2292.

Pazour, G.J., C.G. Wilkerson, and G.B. Witman. 1998. A dynein light chain is essential for retrograde particle movement of intraflagellar transport (IFT). *J. Cell Biol.* 141:979–992.

Pazour, G.J., B.L. Dickert, and G.B. Witman. 1999. The DHC1b (DHC2) isoform of cytoplasmic dynein is required for flagellar assembly. *J. Cell Biol.* 144:473–481.

Piperno, G., and K. Mead. 1997. Transport of a novel complex in the cytoplasmic matrix of *Chlamydomonas* flagella. *Proc. Natl. Acad. Sci. USA*. 94:4457–4462.

Piperno, G., B. Huang, and D.J. Luck. 1977. Two-dimensional analysis of flagellar proteins from wild-type and paralyzed mutants of *Chlamydomonas reinhardtii*. *Proc. Natl. Acad. Sci. USA*. 74:1600–1604.

Piperno, G., M. LeDizet, and X.J. Chang. 1987. Microtubules containing acetylated alpha-tubulin in mammalian cells in culture. *J. Cell Biol.* 104:289–302.

Piperno, G., K. Mead, and S. Henderson. 1996. Inner dynein arms but not outer dynein arms require the activity of kinesin homologue protein KHP1$^{FLA10}$ to reach the distal part of flagella in *Chlamydomonas*. *J. Cell Biol.* 133:371–379.

Piperno, G., E. Siuda, S. Henderson, M. Segil, H. Vaananen, and M. Sassaroli. 1998. Distinct mutants of retrograde intraflagellar transport (IFT) share similar morphological and molecular defects. *J. Cell Biol.* 143:1591–1601.

Porter, M.E., R. Bower, J.A. Knott, P. Byrd, and W. Dentler. 1999. Cytoplasmic dynein heavy chain 1b is required for flagellar assembly in *Chlamydomonas*. *Mol. Biol. Cell.* 10:693–712.

Ramanis, Z., and D.J. Luck. 1986. Loci affecting flagellar assembly and function map to an unusual linkage group in *Chlamydomonas reinhardtii*. *Proc. Natl. Acad. Sci. USA*. 83:423–426.

Rosenbaum, J.L., J.E. Moulder, and D.L. Ringo. 1969. Flagellar elongation and shortening in *Chlamydomonas*: the use of cycloheximide and colchicine to study the synthesis and assembly of flagellar proteins. *J. Cell Biol.* 41:600–619.

Scholey, J.M. 1996. Kinesin-II, a membrane traffic motor in axons, axonemes, and spindles. *J. Cell Biol.* 133:1–4.

Signor, D., K.P. Wedaman, J.T. Orozco, N.D. Dwyer, C.I. Bargmann, L.S. Rose, and J.M. Scholey. 1999. Role of a class DHC1b dynein in retrograde transport of IFT motors and IFT raft particles along cilia, but not dendrites, in chemosensory neurons of living *Caenorhabditis elegans*. *J. Cell Biol.* 147: 519–530.

Struyf, A., M. Hubert, and P.J. Rousseeuw. 1996. Clustering in an object-oriented environment. *J. Statistic. Software.* 1:1–30.

Takeda, S., Y. Yonekawa, Y. Tanaka, Y. Okada, S. Nonaka, and N. Hirokawa. 1999. Left-right asymmetry and kinesin superfamily protein KIF3A: new insights in determination of laterality and mesoderm induction by kif3A$^{-/-}$ mice analysis. *J. Cell Biol.* 145:825–836.

Tigges, M., T. Wittenberg, P. Mergell, and U. Eysholdt. 1999. Imaging of vocal fold vibration by digital multiplane kymography. *Comput. Med. Imaging Graph*. 23:323–330.

Walther, Z., M. Vashishtha, and J.L. Hall. 1994. The *Chlamydomonas FLA10* gene encodes a novel kinesin-homologous protein. *J. Cell Biol.* 126:175–188.